Hydrogen generation via steam reforming of biodiesel: Process optimization and heat integration

Stefan Martin[a], Friedemann Georg Albrecht[a], Pieter van der Veer[b], Dick Lieftink[b], Ralph-Uwe Dietrich[a]

[a]: German Aerospace Center (DLR), Institute of Engineering Thermodynamics
Pfaffenwaldring 38 – 40, 70569 Stuttgart, Germany
[b]: HyGear B.V., P.O. Box 5280, 6802 EG Arnhem, The Netherlands

Corresponding author: Tel.: +49 711 6862 682; fax: +49 711 6862 665; E-mail address: stefan.martin@dlr.de (S. Martin)

Abstract

The present study investigates the distributed generation of hydrogen (50 Nm^3/h) by steam reforming of biodiesel. The system comprises a steam reformer, a water gas shift stage, a pressure swing adsorption unit and a dual fuel burner. Sensitivity analysis with Aspen Plus shows a positive effect on overall system efficiency for high pressure and a low steam-to-carbon ratio. A theoretical maximum efficiency (based on lower heating value) of 78.2 % can be obtained requiring a complex and costly heat exchanger network. Consequently, a system simplification is proposed resulting in a novel fuel processor concept for steam reforming of biodiesel based on a fully heat integrated system. A thermal system efficiency of 75.6 % is obtained at S/C=2.53, p=13 bara and T_{Ref}=825 °C. The techno-economic evaluation reveals hydrogen production costs ranging from 7.25 €/kg to 10.58 €/kg.

Keywords: hydrogen; steam reforming; biodiesel; energy conversion; energy efficiency; techno-economic evaluation

1 Introduction

Today, hydrogen is predominantly produced by steam reforming of natural gas in large-scale, central production plants. However, with an increasing share of fuel cell vehicles (FCVs) in the market, central hydrogen production will suffer from additional costs associated with the distribution of gaseous-phase hydrogen by trailer over long distances (1). In contrast, distributed hydrogen generation (DHG) at fueling stations offers the advantage of using readily available liquid fuels such as diesel and biodiesel with high energy densities and existing infrastructure. DHG is widely seen as a promising alternative in the transition phase towards a fully renewable hydrogen production economy (2, 3, 4). DHG is applicable but not limited to decentralized hydrogen production at fueling sites. There is an increasing demand for annealing applications, in particular for the steel industry and in the production of high quality flat glass. According to Neumann et al. (5) conventional hydrogen generation processes up to 300 Nm^3/h H_2 are being increasingly substituted with advanced steam reforming technologies.

Steam reforming (SR) offers the advantage of high partial pressure of hydrogen in the product gas (70-80 vol.%, dry basis) compared to 40-50 % for autothermal reforming (ATR) and partial oxidation (POX). Taking into account that compressing liquid fuels is less energy intensive than compressing gaseous feeds, steam reforming of liquid fuels is considered to be the preferred option for stationary hydrogen generation (3, 6, 7).

Amongst the available logistic fuels, biodiesel, which is a fatty acid methyl ester (FAME) produced from transesterification of vegetable oil with methanol, appears to be a promising feedstock for DHG by means of SR (8, 9). Biodiesel is a renewable, non-polluting resource with a low sulfur content (typically below 5 ppmw). This renders biodiesel a favorable feedstock for catalytic applications since sulfur is known to be a strong catalyst poison (10).

In the past years, several experimental studies have been conducted shedding light on biodiesel steam reforming (11, 12, 13, 14). Recently, Martin et al. (15) presented a study, the main emphasis of which was placed on finding suitable operating conditions for SR of biodiesel. A stable product gas composition has been achieved over 100 h of operation by using a metallic based precious metal catalyst, applying low feed mass flow rates and a sufficiently high catalyst inlet temperature (> 750 °C). Catalyst deactivation was not observed. A preceding parametric study revealed a detrimental effect of low catalyst inlet temperatures on catalyst deactivation by coking whereas the effect of varying steam-to-carbon (*S/C*) ratio in the considered range (3-5) was negligible. Concurrently, Lin et al. (16) observed increasing carbon formation with decreasing reforming temperature. Regarding the minimum allowable *S/C* ratio in order to ensure coke-free operation, there is evidence from literature data that stable operating conditions with complete biodiesel conversion can be achieved at *S/C* ratios as low as 2 (11, 13).

Moreover, several research groups have carried out theoretical and experimental studies in order to find optimum operating conditions for small-scale hydrogen production targeting high system efficiency and low hydrogen production costs.

Katikaneni et al. (17) carried out a detailed performance study comparing on-site hydrogen generation from liquid fuels by different process routes. Calculations were based on a 1000 kg/d hydrogen filling station (approximately 250 FCVs per day). The hydrogen generation efficiency was found to be highest for a concept based on SR with upstream hydrodesulfurization. For diesel fuel a thermal H_2-efficiency of 65.2 % was calculated. In

terms of hydrogen production costs, the authors conclude that on-site diesel SR is competitive with centralized hydrogen production from natural gas with pipeline transport ($ 6.72 per kg vs. $ 6.23 per kg). Finally, the authors present a hydrogen roadmap starting with a small-scale 50 Nm^3/h H_2 generation system ($ 28.8 per kg H_2), the costs of which can be reduced dramatically by design optimization and heat integration.

T. Persson (18) investigated an integrated 20 kW hydrogen production system based on feedstock methane using a catalytic converter (steam reformer, water gas shift reactor, catalytic burner) and a pressure swing adsorption (PSA) unit. The Aspen Plus calculations were carried out at a pressure of 4 bara assuming a reformer catalyst inlet temperature of 550 °C and an outlet temperature of 850 °C. In the downstream WGS reactor the carbon monoxide content was reduced to below 1.5 vol.%. The PSA off-gas and methane were burned with air at 900 °C in order to provide the necessary heat for the endothermic steam reforming reaction. Parasitic power consumption amounted for 520 W with estimated heat losses of 710 W. The *S/C* ratio and the system pressure were identified to be crucial parameters for achieving a high system efficiency. A maximum theoretical efficiency (based on lower heating value LHV) of 79.1 % is reported at an *S/C* ratio of 2.2.

Hulteberg et al. (3) carried out an experimental investigation based on a similar system using Fischer-Tropsch-Diesel for the production of 7 Nm^3/h H_2. The catalytic converter was operated at a pressure of 5 bara and an *S/C* ratio of 3.1-4.1. Reforming catalyst temperature ranged from 650 °C at the catalyst inlet to 750-800 °C at the catalyst outlet. High heat and mass transfer was ensured by using a noble metal catalyst supported on a patented thermally sprayed woven wire mesh system. With the given experimental set-up, a maximum system efficiency of 58 % (based on LHV) was achieved assuming a parasitic power consumption of 500 W.

Although considerable progress has been made in terms of reformer durability, the development of efficient, low-cost DHG systems based on liquid fuels is still in an early stage leaving room for further development (19, 18). It is well known that hydrogen production costs based on reforming technology depend heavily on the price of the feedstock (20, 1). Thus, improving reforming efficiency is essential in order to make DHG competitive with competing hydrogen production technologies such as central production and distribution by trailer. Moreover, there is a need to substantially reduce investment costs by reducing system size and complexity (4, 21).

Regarding SR of biodiesel, there is no literature data available for heat integrated on-site hydrogen production systems including PSA in the kilowatt range.

The aim of the present paper is to evaluate a 50 Nm^3/h hydrogen generation system based on SR of biodiesel. The main emphasis of this simulation study is placed on maximizing system efficiency by an extensive parameter variation (including system pressure and *S/C* ratio) and setting up a heat exchanger network with a maximum internal heat recovery and a minimum external heating/cooling demand. A novel fuel processor concept is proposed based on a fully heat integrated biodiesel SR system. Further economic analysis is provided.

2 Methodology

A hydrogen generation system based on feedstock biodiesel is evaluated using the commercial software Aspen Plus ®. The thermodynamic equilibrium calculations are based on minimization of Gibbs free energy using the Soave-Redling-Kwong property method (22).

Methyl-oleate ($C_{19}H_{36}O_2$) was chosen as a model substance for biodiesel. Chemically speaking, methyl-oleate is a fatty acid methyl ester produced from transesterification of triolein, the triglyceride of oleic acid, which is known as the dominating fatty acid in vegetable oil (see Fig. 1). Methyl-oleate is considered to be a suitable reference substance for modeling biodiesel SR, since the molar C:H:O-ratio is very similar to biodiesel ($C_{18.3}H_{34.8}O_2$). A more detailed comparison of the physicochemical properties of methyl-oleate and biodiesel is given in (7) and (15).

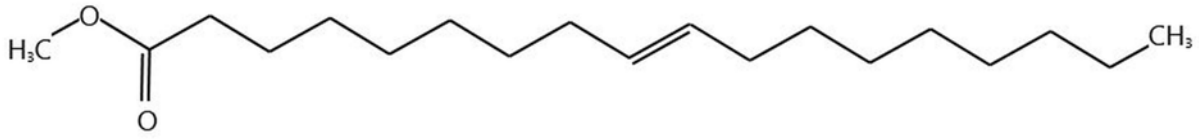

Fig. 1: Chemical structure of biodiesel model substance methyl-oleate ($C_{19}H_{36}O_2$)

SR of methyl-oleate can be described by three linearly independent chemical equations, namely the steam reforming reaction (Eq. (1)), the water-gas shift reaction (Eq. (2)) and the methanation reaction (Eq. (3)). Apart from these main reactions, coking of the catalyst can occur under real-life conditions being favored at low reforming temperatures, low *S/C* ratios and high feed mass flow rates. Thermodynamically, coke formation is not expected at *S/C* ratios higher than 2, the actual value of which depends on the reformer operating conditions (15).

$$C_{19}H_{36}O_2 + 17\ H_2O \rightarrow 19\ CO + 35\ H_2 \qquad \Delta H_{298\,K} = +\ 2\,645\ kJ/mol \qquad (1)$$

$$CO + H_2O \leftrightarrow H_2 + CO_2 \qquad \Delta H_{298\,K} = -\ 41\ kJ/mol \qquad (2)$$

$$CO + 3\ H_2 \leftrightarrow CH_4 + H_2O \qquad \Delta H_{298\,K} = -\ 206\ kJ/mol \qquad (3)$$

The Aspen Plus model consists of a steam reformer (SR), a water gas shift reactor (WGS), a pressure swing adsorption unit (PSA) and a burner (B) (see Fig. 2). The system is operated at pressures higher than 6 bara (up to 13 bara) in order to ensure a high PSA efficiency. The molar *S/C* ratio is varied from 2.5 to 5. All feed streams are supplied at an initial temperature of 20 °C. Water is vaporized and overheated prior to being mixed with biodiesel. By overheating the steam to 400 °C, complete vaporization of the incoming biodiesel is ensured. The water-biodiesel feed stream is then heated up to 650 °C by recuperative heat exchange, making use of the reformate enthalpy. The steam reformer is operated at 825 °C taking into account that coke formation can be significantly reduced by applying high temperatures (15, 16). Upon leaving the reformer section, the hydrogen rich gas is cooled down to a WGS inlet temperature of 300 °C. The WGS reactor is operated in an adiabatic mode resulting in a temperature increase of 50 °C up to 100 °C depending on the actual *S/C* ratio and CO concentration. After leaving the WGS reactor, the gas stream is cooled down to 35 °C leading to a condensation of water. In the PSA unit the gas is divided into pure hydrogen and an off-gas stream containing H_2, CO, CO_2 and CH_4. The PSA unit is implemented as a splitter in Aspen Plus assuming a pressure dependent H_2-efficiency ranging from 55 % at

6 bara to 78.3 % at 13 bara. The remaining heating value of the PSA off-gas is used for the burner, thus providing the necessary heat for the reformer section. The burner is operated in an adiabatic mode, the outlet temperature of which is kept at 1100 °C by adjusting the incoming air mass flow $\dot{m}_{AIR}$. The flue-gas leaves the reformer section at an outlet temperature of 740 °C and can be further used for preheating water and/or air. (Please note that the basic flow-sheet depicted in Fig. 2 is a non-heat integrated system). If the required endothermic heat demand for the steam reforming reaction cannot be met by burning the off-gas with air, additional biodiesel $\dot{m}_{BD-B}$ is fed to the burner. At a given *S/C* ratio, the targeted hydrogen output of 50 Nm^3/h is ensured by adjusting the feed mass flow $\dot{m}_{BD-REF}$ accordingly. A brief overview of the boundary conditions (based on experimentally derived values from a 50 Nm^3/h hydrogen production system developed within the FCH JU project NEMESIS2+ (23)) is given in Tab. 1.

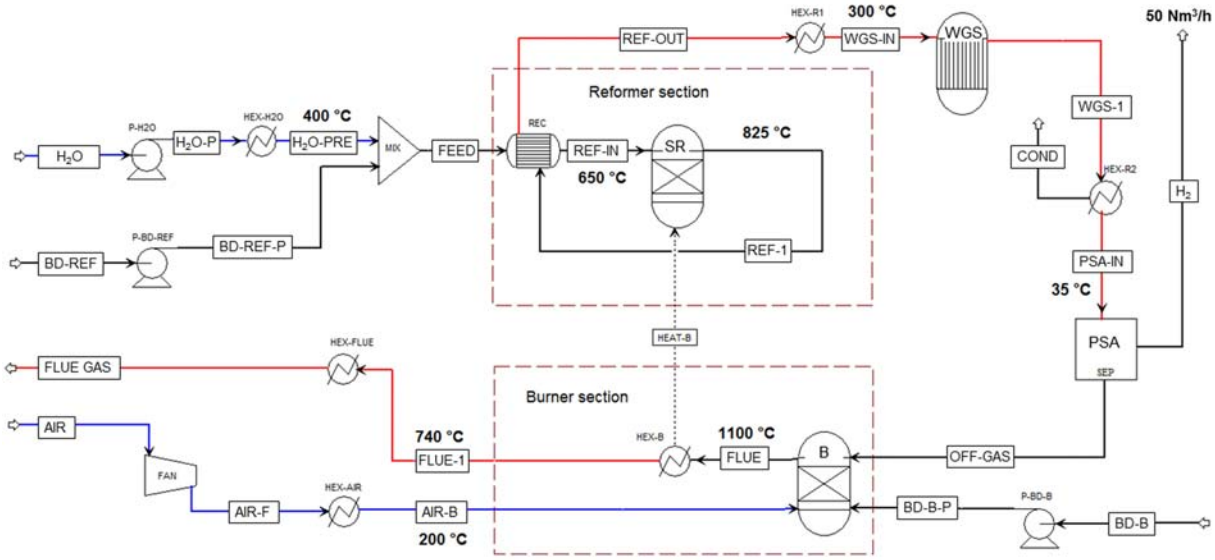

Fig. 2: Basic, non-heat integrated Aspen Plus flow-sheet of a 50 Nm^3/h hydrogen production system based on biodiesel feedstock

Tab. 1 – Boundary conditions of basic Aspen Plus flow-sheet	
Reformer	T_{REF-IN}=650 °C, T_{REF-1}=825 °C
WGS	T_{WGS-IN}=300 °C (adiabatic operation)
PSA	H_2-efficiency: 55 % at 6 bara - 78.3 % at 13 bara
Burner	T_{FLUE}=1100 °C (adiabatic operation)
Flue Gas (after heat release to reformer)	T_{FLUE-1}=740 °C
Steam	$T_{H2O-PRE}$=400 °C
Air	T_{AIR-B}=200 °C (reference case)
H_2 output	50 Nm^3/h

The thermal system efficiency is defined as follows:

$$\eta_{Syst} = \frac{\dot{m}_{H_2} \cdot LHV_{H_2}}{\dot{m}_{BD-REF} \cdot LHV_{BD-REF} + \dot{m}_{BD-B} \cdot LHV_{BD-B}} \quad (4)$$

LHV: lower heating value; $\dot{m}_{H2}$: hydrogen product mass flow; $\dot{m}_{BD-REF}$: biodiesel mass flow to the reformer; $\dot{m}_{BD-B}$: biodiesel mass flow to the burner

For the given system, the numerator of Eq. 4 is constant as the hydrogen output is fixed at 50 Nm^3/h. Thus, the thermal system efficiency can be calculated from the biodiesel demand for the reformer and the burner. An additional electrical power demand P_{el} is needed for cooling the WGS outlet stream to the required PSA inlet temperature as well as for the biodiesel and water pump and the air blower. Heat and pressure losses are not considered within this study.

The flow-sheet depicted in Fig. 2 comprises two streams that have to be heated up (=cold streams) according to the process specifications, namely “H2O-P” to “H2O-PRE” and “AIR-F” to “AIR-B” and three streams which are cooled down (=hot streams), namely “FLUE-1” to “FLUE GAS”, “REF-OUT” to “WGS-IN” and “WGS-1” to “PSA-IN”. Using the enthalpy of the hot streams for heating up the cold streams is decisive in optimizing the net system efficiency.

In this work, a systematic approach is followed by applying Pinch analysis in order to achieve proper heat integration. For given process parameters, hot and cold streams are combined to so-called hot and cold composite curves. Based on the choice of an appropriate ΔT_{min} (=minimum temperature difference between hot and cold composite curves, here: 15 °C), the maximum achievable heat recovery within the system and the energy targets for hot and cold utilities can be derived directly from the composite curves. It is thereby always possible to set up a heat exchanger network that fulfills the energy targets (minimum utility targets and maximum heat recovery). For a more detailed description of the widely used Pinch method please refer to (24).

Techno-economic analysis

A techno-economic evaluation of hydrogen net production costs (NPC) is conducted. The cost estimation complies with a class three estimate of AACE International (25) corresponding to an expected accuracy of +- 30 %. All monetary flows were converted to Euro and 2014 prices.

In a first step, total capital investment (TCI) was calculated taking into account equipment costs and further capital requirements for unit installation, instrumentation and control, piping system, electrical systems and contingency. Equipment costs of steam reformer, WGS, PSA and burner are based on experience from the NEMESIS2+ project and vendors’ quotations for reactor vessels and the catalyst. Cost data from literature (26) were used to estimate costs for heat exchangers, pumps and compressors. Scaling and experience curve effects, inflation, pressure and material factors were accounted for as shown in Eq. (5) adapted from (26), (27) and (28).

$$EC_n = EC_{ref} \cdot \left(\frac{s}{s_{ref}} \right)^d \cdot \left(\frac{CEPCI_{2014}}{CEPCI_{ref}} \right) \cdot F_{pre} \cdot F_{mat} \cdot (1-L)^{\log_2(n)} \quad (5)$$

$$TCI = \sum_{i=1}^{m} EC_i \cdot \left(1 + \sum_{j=1}^{5} F_{eco,j}\right) \quad (6)$$

EC_n are the equipment costs for the n[th] manufactured unit. EC_{ref} and s_{ref} are the equipment costs and capacity of the reference component, d is the scale factor, $CEPCI$ the used chemical engineering plant cost index (29) and F_{pre} and F_{mat} are optional pressure and material factors, respectively. L is the experience rate and n the total number of manufactured reformer units. An experience rate between 10 % and 20 % was assumed for the used technology meaning that unit production costs are reduced by 10 % to 20 %, when the total volume of manufactured units is doubled (28, 30). Total capital costs were calculated according to Eq. (6). Cost requirements for equipment installation, instrumentation and control, piping system and electrical systems were considered by multiplying purchased equipment costs by pre-defined ratio factors $F_{eco,j}$. The annuity method of depreciation was used to calculate annual capital requirements.

Operational costs consist of expenses on biodiesel and utilities (electricity, feed water). Annual costs for maintenance, insurances & taxes and working capital were expected to be approximately 4.5 %, 2 % and 10 % of TCI, respectively. Labor costs were estimated assuming 300 man hours per year at gross labor costs of 37.32 €/h (31). All relevant parameters for the techno-economic evaluation are given in Table 2.

Tab. 2 – Parameters for economic evaluation

Plant specifications and utility prices (2014)			**Economic factors**		
Plant service life:	**20**	*years*	Interest rate:	**7**	*% on TCI*
Annual full load hours:	**8640** [a]	*h/year*	Installation factor:	**25**	*% of EC*
			Instrumentation and control:	**22**	*% of EC*
Total man hours per year:	**300**	*h/year*	Piping system:	**5**	*% of EC*
Gross labor costs:	**37.32** [31]	*€/h*	Electrical system:	**10**	*% of EC*
			Contingency:	**16**	*% of EC*
Electricity price:	**0.139** [32]	*€/kWh*	Maintenance:	**4.5**	*% of TCI*
Clean water:	**1.71** [33]	*€/m³*	Insurances & taxes:	**2**	*% of TCI*
Biodiesel (with taxes):	**1.36** [34,35]	*€/l*	Working capital	**10**	*% of TCI*

a) corresponding to 360 days in operation and 5 days required for annual shutdown/maintenance

3 Results and Discussion

3.1 Non-heat-integrated system: Effect of pressure on system efficiency

Based on the 50 Nm^3/h non-heat integrated Aspen Plus flow-sheet (Fig. 2) a sensitivity analysis has been carried out at *S/C*=5 by varying system pressure from 6 bara to 13 bara. As can be seen from Fig. 3 the hydrogen efficiency as defined by Eq. 4 increases from 53.9 % at 6 bara to 62.4 % at 13 bara which is mainly attributed to an improved PSA-efficiency resulting in a decreased amount of biodiesel fed to the reformer ($\dot{m}_{BD-REF}$). Despite

a slight increase of the required biodiesel mass flow to the burner $\dot{m}_{BD-B}$ - which arises from the fact that the PSA off-gas heat load (based on LHV) drops from 127.2 kW at 6 bara to 48.3 kW at 13 bara (see Fig. 4a) - total fuel consumption is reduced from 26.4 kg/h to 22.8 kg/h. The drop of the PSA off-gas heat load is mainly caused by a rapid decrease of the off-gas mass flow and an increased share of CO_2 (Fig. 4b). Obviously, applying high pressure is beneficial for the given H_2 generation system including a PSA unit.

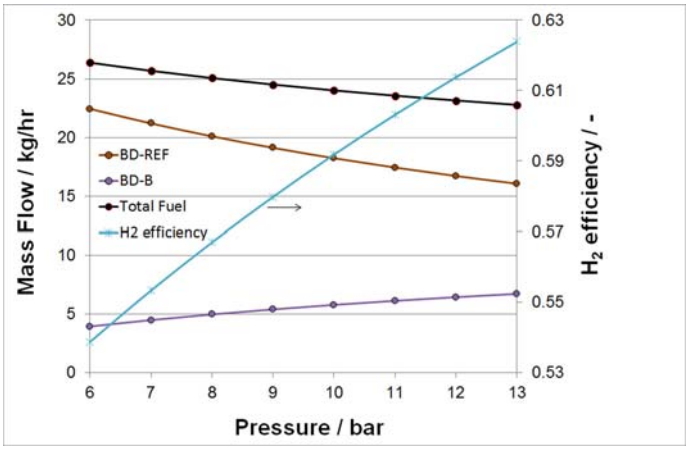

Fig. 3: Effect of system pressure on mass flows and H_2 efficiency

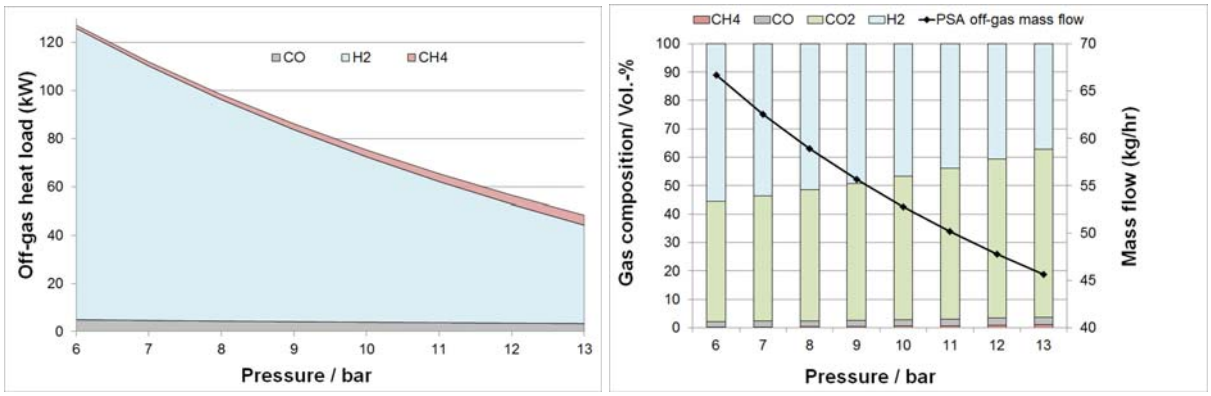

Fig. 4: Effect of system pressure on PSA off-gas heat load (Fig. 4a), PSA off-gas composition and PSA off-gas mass flow (Fig. 4b)

Assuming an operating pressure of 13 bara and *S/C*=5 as a starting point (=operating regime "0"), the hydrogen efficiency can be further improved by increasing the burner air preheating temperature T_{AIR-B} (Fig. 5a). By doing so, less fuel $\dot{m}_{BD-B}$ is needed for the burner in order to provide the necessary heat for the endothermic reforming reaction (Fig. 5b), while the amount of fuel needed for the reformer $\dot{m}_{BD-REF}$ remains unaffected. Accordingly, the H_2 efficiency (Eq. 4) rises.

3.2 Heat-integrated system

3.2.1 Maximum achievable air preheating temperature at different S/C-ratios

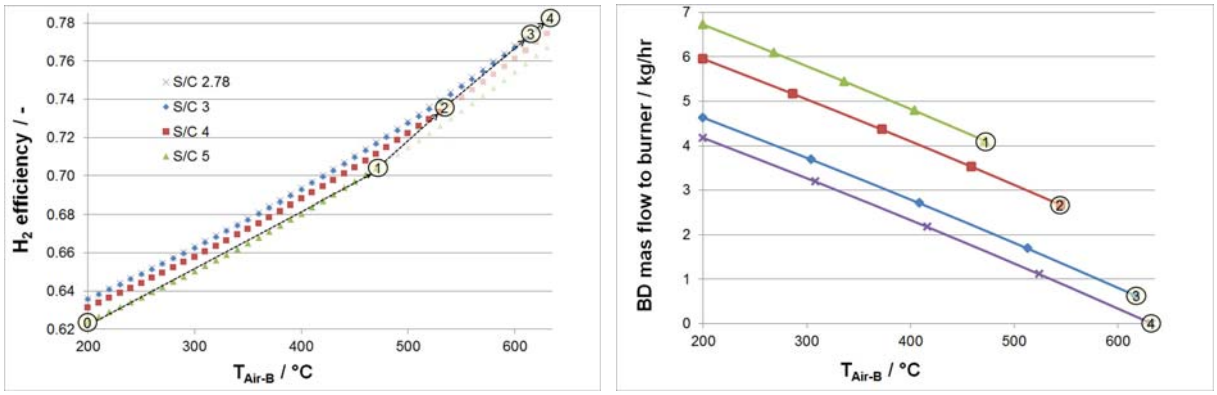

Fig. 5: Effect of *S/C* ratio and air preheating temperature $T_{AIR\text{-}B}$ on H_2 efficiency as defined by Eq. 4 (Fig. 4a) and required biodiesel mass flow to burner (Fig. 4b). Operating regimes 1, 2, 3 and 4 (yellow-filled circles) represent the maximum achievable preheating temperatures for heat integrated systems.

Regarding a heat integrated system without additional external heating demand (except fuel demand for burner), the achievable preheating temperature $T_{AIR\text{-}B,max}$ (yellow-filled circles in Fig. 5) is limited by the enthalpy loads and related temperature levels of the available residual heat streams. For a given S/C-ratio, the maximum preheating temperature $T_{AIR\text{-}B,max}$ can be derived from the composite curves, which is graphically shown in Fig. 6. The composite curves that give the maximum allowable preheating temperature $T_{AIR\text{-}B,max}$ are obtained iteratively by targeting a minimum temperature approach ΔT_{min} between the hot and cold composite curves with no additional external heating demand ($\dot{Q}_{heat} = 0$).

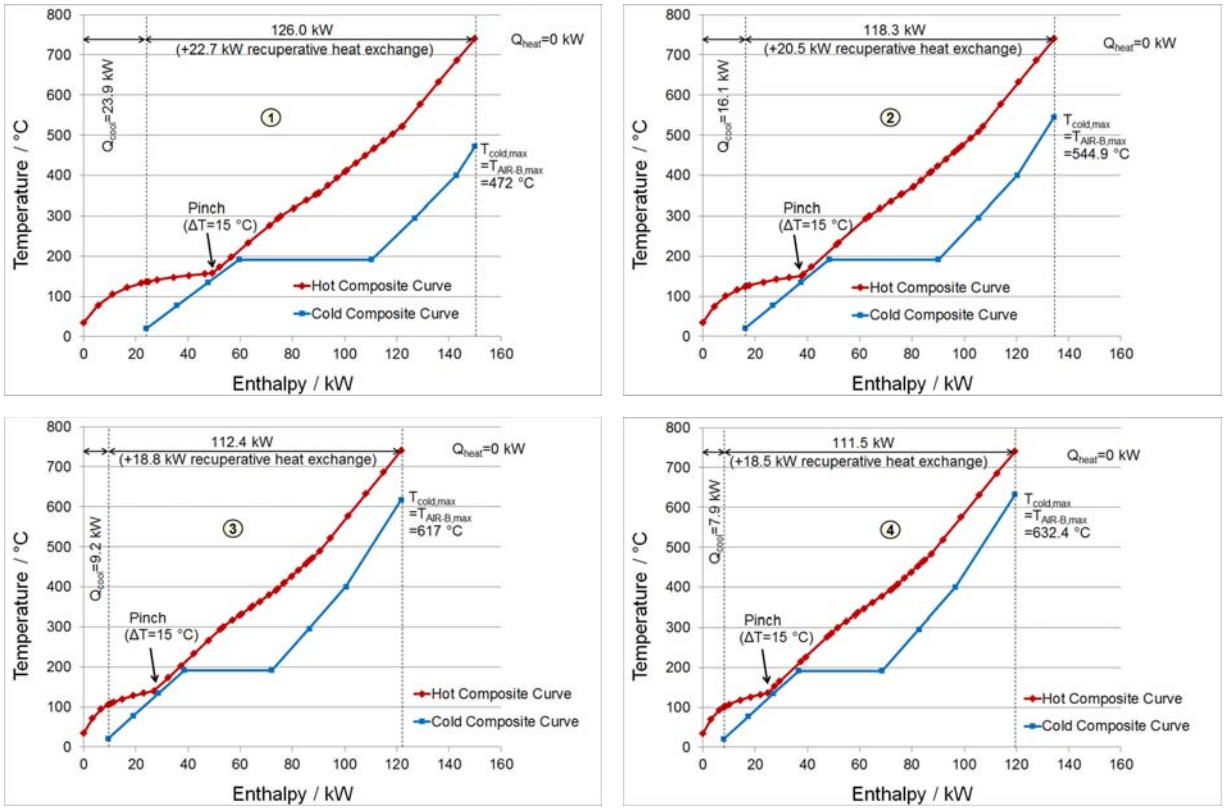

Fig. 6: Hot and cold composite curves of basic Aspen Plus flow-sheet (upper left: *S/C*=5 corresponding to operating regime 1, upper right: *S/C*=4, corresponding to operating regime 2, bottom left: *S/C*=3 corresponding to operating regime 3, bottom right: *S/C*=2.78 corresponding to operating regime 4)

As can be seen exemplarily from Fig. 6a, the maximum achievable air preheating temperature $T_{AIR\text{-}B,max}$ at *S/C*=5 is 472 °C. By lowering the *S/C* ratio stepwise to 4, 3 and 2.78 $T_{AIR\text{-}B,max}$ can be raised from 472 °C to 545 °C, 617 °C and 632 °C, respectively. At this point (operating regime 4, Fig 6c), hereinafter referred to as the *thermo-neutral* point, no additional fuel is needed for the burner ($\dot{m}_{BD-B}$ =0). The necessary heat for the endothermic reforming reaction is provided solely by the heating value of the PSA off-gas. From a technical point of view, this is highly advantageous since it eliminates the need of a dual fuel burner. Instead, a conventional gas burner can be used.

Moreover, Fig. 6 reveals an increasing energy turnover at higher *S/C*. Both the internal heat recovery and the external cooling demand increase (internal heat recovery: from 111.5 kW at *S/C*=2.78 to 126.0 kW at *S/C*=5, external cooling demand: from 7.9 kW at *S/C*=2.78 to 23.9 kW at *S/C*=5) resulting in a larger and more costly heat exchanger (HEX) network and increased energy costs.

3.2.2 Effect of S/C-ratio on system efficiency

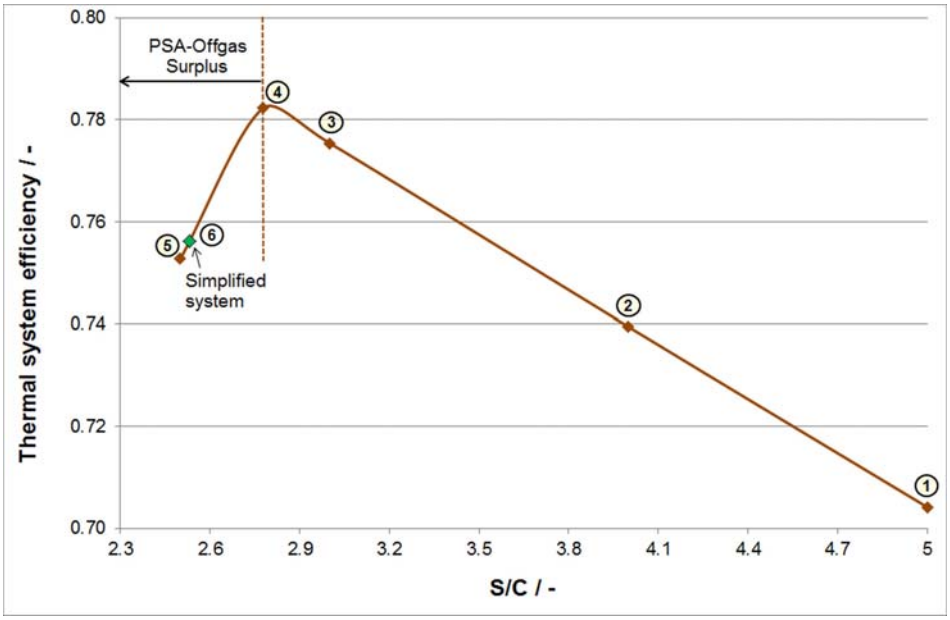

Fig. 7: Thermal system efficiency (as defined by Eq. 4) as a function of *S/C*

The thermal system efficiency (as defined by Eq. 4) that corresponds to the maximum achievable air preheating temperature of an heat integrated system increases linearly with decreasing *S/C*-ratio (Fig. 7) up to the thermo-neutral point (operating regime 4) where PSA-off-gas starts to emerge. A maximum theoretical net H_2 efficiency of 78.2 % is obtained. Obviously, if the PSA off-gas surplus is vented, the net H_2 efficiency declines (operating regime 5). One could think about partly recycling the PSA off-gas, resulting in a further efficiency rise. However, this is a rather theoretical consideration as recycling the PSA off-gas would require gas compression from 1 bara to 13 bara. Taking into account that compressing gaseous feeds is energy intensive and considering that the PSA recycle ratio becomes extraordinary high at low *S/C*, the option of recycling the PSA off-gas was discarded. Tab. 3 gives an overview of the process characteristics of the considered operating regimes. The hydrogen output is kept constant at 50 Nm^3/h for all operating regimes.

	Tab. 3 – Process characteristics of different operating regimes						
Operating regime	*S/C*	T_{AIR-B} (°C)	$\dot{m}_{BD-REF}$ (kg/h)	$\dot{m}_{BD-B}$ (kg/h)	$\dot{m}_{BD,total}$ (kg/h)	η_{Syst} (%)	P_{el} (kW)
0	5.00	200.0	16.06	6.72	22.78	62.4	8.11
1	5.00	472.0	16.06	4.11	20.17	70.4	6.19
2	4.00	544.9	16.56	2.67	19.23	73.9	5.70
3	3.00	617.0	17.72	0.63	18.35	77.5	5.32
4	2.78	632.4	18.17	0.00	18.17	78.2	5.26
5	2.50	642.2	18.88	0.00	18.88	75.3	5.26
6	2.53	570.0	18.79	0.00	18.79	75.6	5.82

Considering the substantially reduced total fuel consumption (Tab. 3) low *S/C* ratios appear highly favorable for heat-integrated DHG systems. The higher system efficiency at lower *S/C* mainly arises from the reduced heat demand for preheating and vaporization of water.

As mentioned above, the highest theoretical H_2 net efficiency is obtained under thermo-neutral conditions at *S/C*=2.78. Nonetheless, a heat integrated system based on these conditions would require a complex HEX network including several stream splits. In particular, the narrow section right above the pinch point and the initiation of water condensation during cooling of the “WGS-1”-stream is detrimental to building up a HEX network. Even though we know from pinch theory that it is theoretically possible to set up a HEX network fulfilling the energy targets based on the composite curves at thermo-neutral conditions, the practicability of such a system must be questioned. Therefore we decided to simplify the system by limiting the use of the “WGS-1”-temperature (for heat integration purposes) to 132 °C, which is the dew-point of the respective stream.

3.2.3 Heat exchanger network of simplified system

The hot and cold composite curves of the simplified system (operating regime 6) are depicted in Fig. 8.

The targeted minimum temperature approach between the hot and cold composite curve is 67 °C. 120.5 kW (102.1 kW + 18.4 kW) can be recovered within the system. The biodiesel mass flow to the burner can be eliminated (see Tab. 3) since the heating value of the PSA off-gas is sufficient for providing the necessary heat for the reforming reaction. Compared to operating regime 4, a slightly lower *S/C* has to be applied in order to ensure thermo-neutral conditions (*S/C*=2.53 compared to *S/C*=2.78).

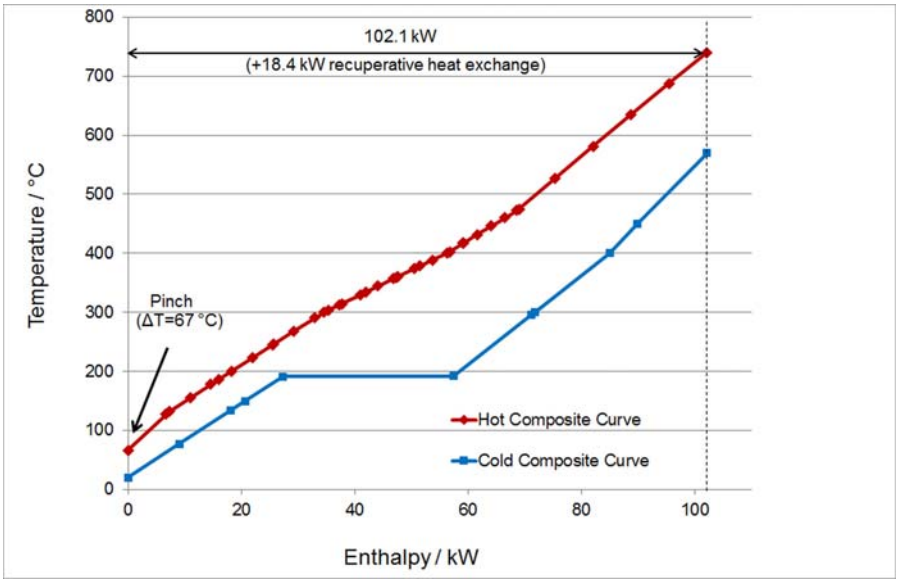

Fig. 8: Composite curves of the simplified hydrogen generation system (operating regime 6)

Based on the composite curves of the simplified system, a HEX network has been set up targeting a maximum internal heat recovery with no additional external heating/cooling demand (except the cold utility which is required to cool down the WGS product gas stream from dew point temperature to the PSA inlet temperature). The fully heat integrated system is depicted in Fig. 9.

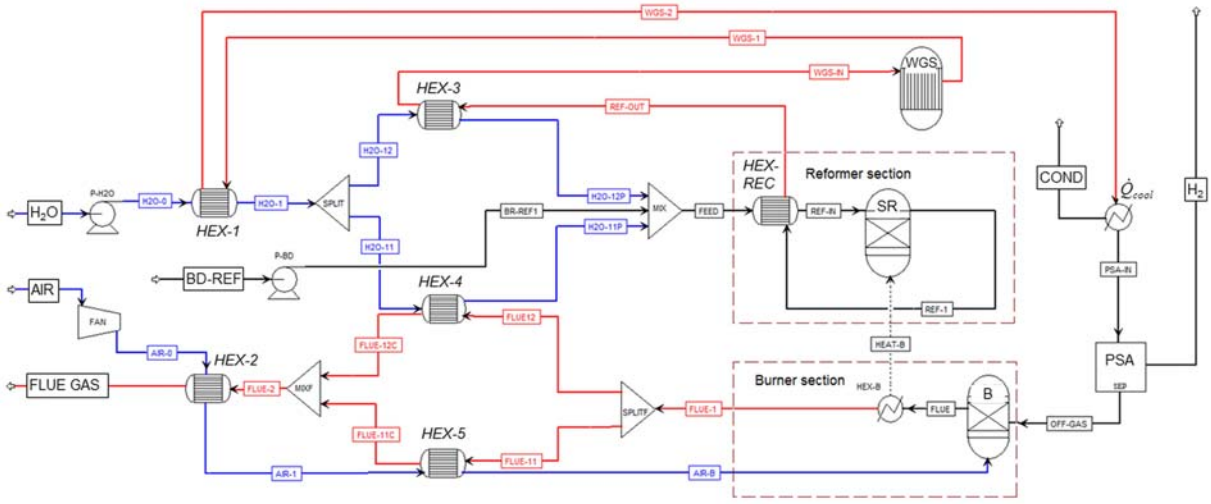

Fig. 9: Heat integrated 50 Nm^3/h hydrogen generation system based on SR of biodiesel

18.79 kg/h of biodiesel are consumed in order to generate 50 Nm^3/h (4.436 kg/h) of hydrogen. The system is operated at *S/C* 2.53 thus eliminating the need of feeding additional biodiesel to the burner. The endothermic heat demand for the steam reformer (47.6 kW) is provided by the burner making use of the PSA off-gas. By splitting up the flue-gas stream "FLUE-1", the incoming air stream "AIR-1" is preheated to 570 °C ("AIR-B") before entering the burner. The water stream "H2O-1" is split up similarly, one stream being heated up to 400 °C by making use of the "FLUE-12"-stream, the other stream being heated up to 400 °C by transferring waste heat from the "REF-OUT"-stream. Preheating of water ("H2O" to "H2O-1") is achieved by cooling down stream "WGS-1" to dew point temperature. The system

produces 5,391 l/h of hydrogen at 10 bara delivery pressure (corresponding to 50 Nm^3/h H_2 at standard conditions).

The feed and product stream characteristics as well as the heat exchanger properties of the proposed fuel processor concept including the electrical power demand P_{el} are depicted in Tab. 4 and 5. In line with the energy targets derived from the composite curves of the simplified system (see Fig. 8), 120.5 kW are recovered within the system by matching cold and hot streams. An additional electrical energy demand of 5.82 kW is required. Although the minimum temperature approach is slightly lower than targeted (18.8 °C versus 67 °C), a near-optimal HEX network is obtained with a thermal system efficiency (as defined by Eq. 4) of 75.6 %.

Tab. 4 – Feed and product stream characteristics of heat integrated system

	H2O	BD-REF	AIR	FLUE-OUT	COND	H2
$\dot{m}$ (kg/h)	54.9	18.8	335.4	384.0	20.6	4.436
$\dot{V}$ (l/h)	55.0	21.6	282,130	365,994	21.8	5,391
T (°C)	20	20	20	65.3	20	20

Tab. 5 – Heat exchanger properties ($\dot{Q}$: transferred heat; A: heat exchanger area; $\Delta T_{\min}$: minimum temperature approach), electrical power demand P_{el} : 5.82 kW

	HEX-1	HEX-2	HEX-3	HEX-4	HEX-5	HEX-REC
$\dot{Q}$ (kW)	13.24	16.06	8.65	26.51	37.66	18.36
A (m^2)	0.90	123.9	0.85	11.2	126.5	1.71
$\Delta T_{\min}$	112.0	20.5	74.9	18.8	20.5	175.0

3.3 Techno-economic analysis

3.3.1 Total hydrogen net production costs (NPC)

NPC were calculated based on the optimized reformer concept presented in Fig. 9 and the economic factors and assumptions presented in Table 2. For the first produced reformer unit, total equipment costs amount to 442,031 €. The most expensive equipment is the biodiesel reformer followed by the installed burner and the PSA, which accounts for approximately 45.8 %, 18.7 % and 18.0 % of total equipment costs, respectively. A breakdown of equipment costs is shown in the left pie chart in Fig. 10.

Based on annual capital cost requirements and current market prices for raw materials, utilities and labor costs in Germany, total hydrogen production costs of 10.58 €/kg H_2 were estimated. Thereby, expenses for biodiesel accounts for more than 63 % of NPC indicating that the economic feasibility of the presented reformer concept is highly depending on biodiesel market prices. Annual capital costs are the second largest cost item, though, with a share of 17.83 % capital costs have by far not the same impact on NPC compared to the

biodiesel price. Expenses for labor, taxes and insurances have a small effect on H_2 production costs. NPC broken down by cost items are shown in the right pie chart in Fig. 10.

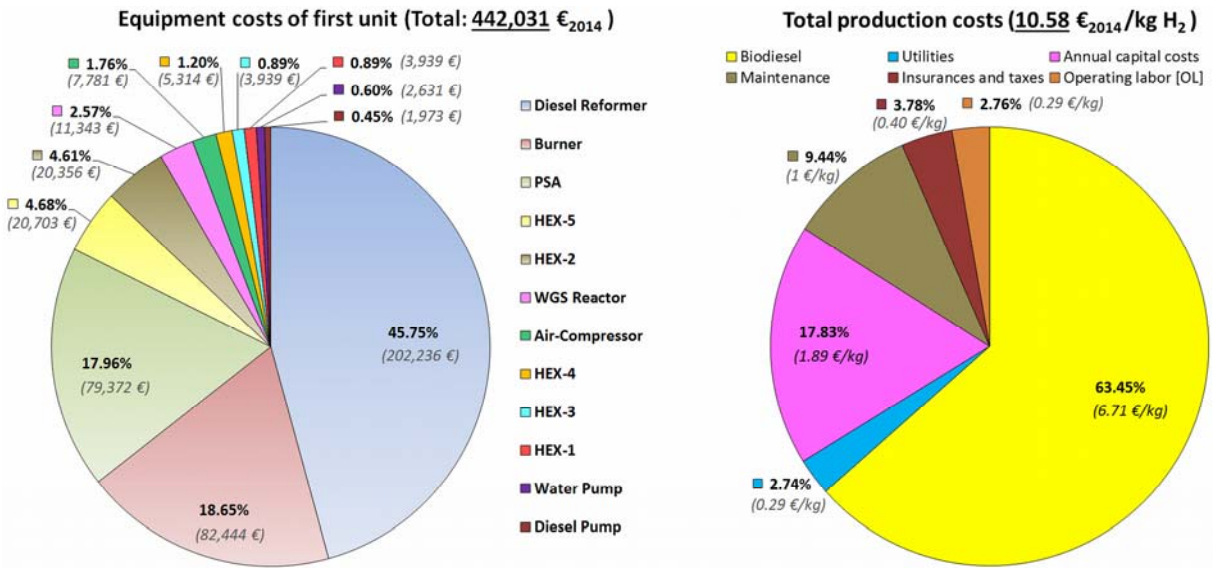

Fig. 10: Equipment costs and total hydrogen production costs of first produced reformer unit

It is worth noticing that the relative high biodiesel market price is due to the consideration of taxes. In some European countries, hydrogen and the raw materials used in the production process are tax free. As a consequence, significant lower hydrogen production costs are obtained. When neglecting taxes on biodiesel, total hydrogen production costs of 7.30 €/kg were calculated for the presented case.

3.3.2 Experience curve effects

Especially for new developed technologies, equipment costs as well as labor costs for installation and maintenance are decreasing between the first-of-a-kind (FOAK) and N^{th}-of-a-kind unit (NOAK) (28). In order to account for expected cost reductions regarding equipment costs (including installation and maintenance), change of hydrogen production costs was analyzed assuming different experience rates L in Eq. (6). Since it is not possible to determine the exact experience rate for the presented reformer concept at the current technological level, L was varied between 10 % and 20 %, which is a typical range for newly developed technologies. Results for the first 100 manufactured units are presented in Fig. 11.

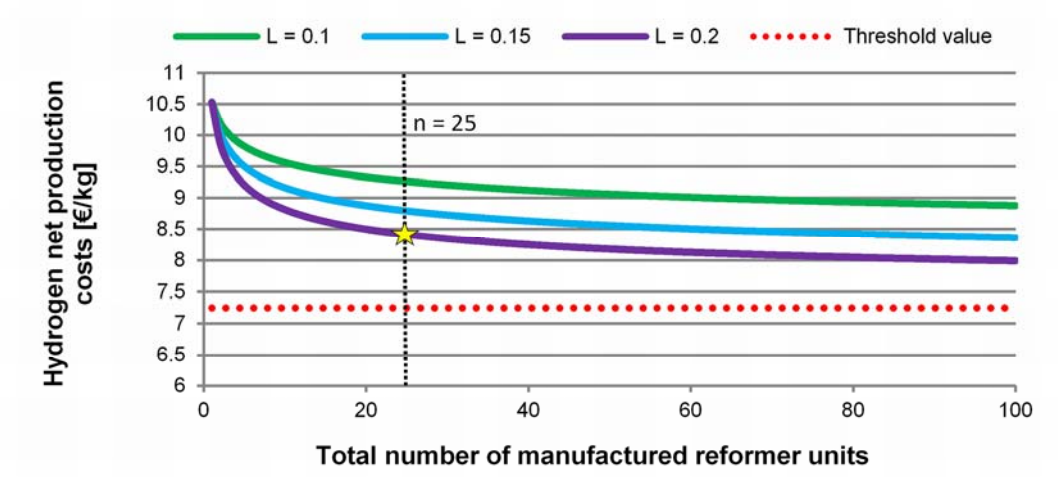

Fig. 11: Development of hydrogen net production costs taking into account experience curve effects

In general, NPC of hydrogen decrease with every manufactured unit. However, the largest cost reduction effect can be seen in the range between 1 and 25 manufactured units, whereupon NPC tends to a threshold value indicated by the red dashed line in Fig. 11. When reaching the threshold value, capital costs are close to zero and NPC only consists of expenses for biodiesel, utilities and labor costs. At this point, reducing hydrogen production costs is only possible by reducing operational costs or by increasing the energetic efficiency of the reformer concept.

For the given case, the threshold value is 7.25 €/kg corresponding to a maximum cost reduction potential of 31.5 %. Assuming an experience rate of 10 % and 20 %, NPC of hydrogen is reduced by 12.5 % and 20.5 % (9.26 and 8.46 €/kg) for the 25th unit and 16 % and 24 % (8.88 and 8 €/kg) for the 100th unit, respectively.

3.3.3 Sensitivity analysis

The impact on NPC of the three most relevant cost items (biodiesel price, annual capital costs and maintenance) as well as the electricity price was investigated in a sensitivity analysis. Especially biodiesel prices can vary significantly over time due to changes of global oil prices or legal and fiscal framework conditions. In order to take experience curve effects into account, sensitivity analysis was carried out for the 25th manufactured reformer unit assuming an experience rate of 20 % (This case is marked with a yellow star in Fig. 11). Starting from initial NPC of 8.46 €/kg, costs and prices were varied within a range of -/+ 40 %. Results are presented in Fig. 12.

By varying biodiesel prices, hydrogen production costs are considerably affected and amount to 5.77 €/kg and 11.15 €/kg for 40% lower and higher market prices, respectively. Changes in equipment costs have a less significant impact with NPC ranging from 8 to 8.93 €/kg. Since accuracy of a AACE class three cost estimation of equipment costs lies within +- 30 %, it is worth noticing that by definition NPC can likely be in the range between 8.1 and 8.81 €/kg. Maintenance and electricity costs have a negligible effect on hydrogen production costs.

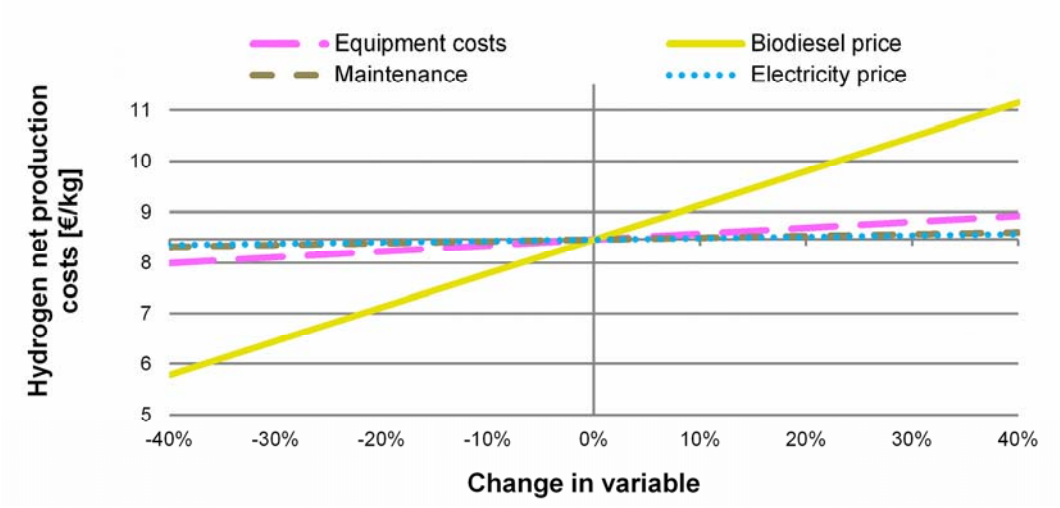

Fig. 12: Results of sensitivity analysis of 25th unit

3.3.4 Comparison of basic and optimized system

Finally, the economic performance of the basic, non-heat integrated system (Fig. 2) and optimized, heat integrated reformer system (Fig. 9) shall be discussed. Figure 13 presents net hydrogen production costs for the first and 25th manufactured unit broken down in relevant cost items.

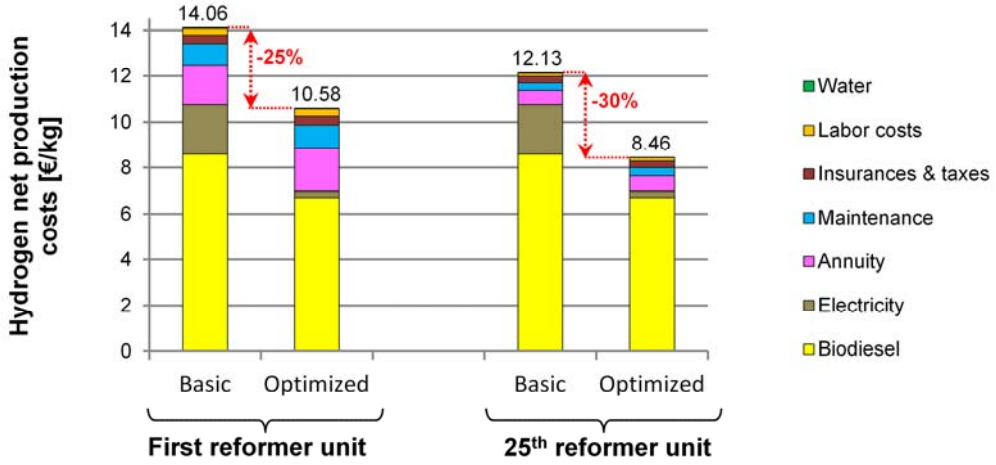

Fig. 13: Comparison of hydrogen production costs based on basic, non-heat integrated and optimized, heat integrated reformer system

Without process optimization and heat integration, significantly more biomass and electricity is required per kg of hydrogen produced resulting in high NPC of 14.06 €/kg for the first reformer unit. Although equipment costs are approximately 9% higher in the optimized reformer concept due to integration of several heat exchangers, total production costs are 25% lower (10.58 €/kg). Especially the electricity consumption is considerably reduced, since internal heating demand is minimized. As a result, it can be stated that the drawback of higher equipment costs in the optimized system is by far outweighed by significant lower operational costs.

When taking experience curve effects into account, the hydrogen production costs are even more reduced as shown for the 25th manufactured unit. This is due to the fact that fixed capital costs are reduced whereas operational costs remain unaffected. Thus, optimizing the system results in more than 30% lower hydrogen production costs.

4 Conclusions

This study serves to evaluate a 50 Nm^3/h hydrogen generation system based on steam reforming of biodiesel. Results show that it is vital in terms of improving system efficiency to apply a high system pressure and a low *S/C* ratio. The positive effect of pressure predominantly arises from an increased PSA efficiency at high pressures, which outweighs the adverse effect of thermodynamics (lower syngas yield at high pressure). The upper limit of the system pressure is hardware-dependent whereas the lower limit of the *S/C* ratio is determined by the so called *thermo-neutral* point. At this point, the heat for the steam reforming unit can be provided exclusively by burning the off-gas from the PSA, thus eliminating the need of a dual fuel burner. Further lowering the *S/C* ratio is not advisable since a PSA off-gas surplus starts to emerge, resulting in a decrease in the net system efficiency. Moreover, a low *S/C* ratio increases the risk of coke formation on the catalyst surface. Regarding practical applications a trade-off between high catalyst durability and high system efficiency must be found.
Based on the results of the process optimization, proper heat integration of the system has been carried out resulting in a near-optimal HEX network with a net system efficiency of 75.6 % (based on LHV). Techno-economic analysis of the heat integrated fuel processor system based on steam reforming of biodiesel reveals a major impact of biodiesel price on hydrogen net production costs. 8.46 €/kg were calculated for the 25th reformer unit, the costs of which can be further brought down by increasing the number of units and/or increasing the unit size.

Acknowledgement

The authors gratefully acknowledge the support of the Fuel Cells and Hydrogen Joint Undertaking (FCH JU) under Grant Agreement No. 278138. For proofreading the manuscript we thank Martin Kraenzel.

References

[1] G.T. Yeh, Y.L. Kao, S.Y. Yang, M.H. Rei, Y.Y. Yan, P.C. Lee, Low cost compact onsite hydrogen generation, Int J Hydrogen Energ 39 (2014) 20614-20624

[2] I. Schjølberg, C. Hulteberg, I. Yasuda, C. Nelsson, Small scale reformers for on-site hydrogen supply, Energy Procedia 29 (2012) 559-566

[3] P.C. Hulteberg, H. Burford, K. Duraiswamy, B. Porter, R. Woods, A cost effective steam reformer for a distributed hydrogen infrastructure, Int J Hydrogen Energ 33 (2008) 1266-1274

[4] J.M. Ogden, Review of small stationary reformers for hydrogen production, Princeton University Center for Energy and Environmental Studies, Report for the International Energy Agency, Task 16 (2001) 1-49

[5] P. Neumann, F. von Linde, Options for economical supply of hydrogen, MPT International 2 (2003) 72-75

[6] J.D. Holladay, J. Hu, D.L. King, Y. Wang, An overview of hydrogen production technologies, ChemCatChem 3 (2011) 244-260

[7] S. Martin, A. Wörner, On-board reforming of biodiesel and bioethanol for high temperature PEM fuel cells: Comparison of autothermal reforming and steam reforming, J Power Sources 196 (2011) 3163-3171

[8] A. Qi, B. Peppley, K. Karan, Integrated fuel processors for fuel cell application: A review, Fuel Process Technol 88 (2007) 3-22

[9] G. Nahar, V. Dupont, Hydrogen via steam reforming of liquid biofeedstock, Biofuels 3 (2012) 167-191

[10] C.H. Bartholomew, R.J. Farrauto, Fundamentals of Industrial Catalytic Processes, Wiley (2006), Second Edition

[11] N. Abatzoglou, C. Fauteux-Lefebvre, N. Braidy, Biodiesel reforming with a $NiAl_2O_4/Al_2O_3$-YSZ catalyst for the production of renewable SOFC fuel, WIT Transactions on Ecology and the Environment 143 (2011) 145-155

[12] Y. Shiratori, T. Quang-Tuyen, Y. Umemura, T. Kitaoka, K. Sasaki, Paper-structured catalyst for the steam reforming of biodiesel fuel, Int J Hydrogen Energy 38 (2013) 11278-11287

[13] Y. Shiratori, T. Quang-Tuyen, K. Sasaki, Performance enhancement of biodiesel fueled SOFC using paper-structured catalyst, Int J Hydrogen Energy 38 (2013) 9856-9866

[14] G. Nahar, V. Dupont, M.V. Twigg, E. Dvininov, Feasibility of hydrogen production from steam reforming of biodiesel (FAME) feedstock on Ni-supported catalysts, Appl Catal B-Environ 168-169 (2015) 228-242

[15] S. Martin, G. Kraaij, T. Ascher, D. Wails, A. Wörner, An experimental investigation of biodiesel steam reforming, Int J Hydrogen Energ 40 (2015) 95-105

[16] J. Lin, T.A. Trabold, M.R. Walluk, D.F. Smith, Bio-fuel reforming for solid oxide fuel cell applications. Part 2: Biodiesel, Int J Hydrogen Energ 39 (2014) 183-195

[17] S.P. Katikaneni, F. Al-Muhaish, A. Harale, T. V. Pham, On-site hydrogen production from transportation fuels: An overview and techno-economic assessment, Int J Hydrogen Energ 39 (2014) 4331-4350

[18] T. Persson, Simulation of small-scale hydrogen production, Department of Chemical Engineering Lund University, master thesis (2007)

[19] S. Specchia, Fuel processing activities at European level: A panoramic overview, Int J Hydrogen Energ 39 (2014) 17953-17968

[20] P. Bolat, C. Thiel, Hydrogen supply chain architecture for bottom-up energy systems models. Part 2: Techno-economic inputs for hydrogen production pathways, Int J Hydrogen Energ 39 (2014) 8898-8925

[21] I. Dincer, C. Acar, Review and evaluation of hydrogen production methods for better sustainability, Int J Hydrogen Energ (2014), Article in Press

[22] G. Soave, Equilibrium constants from a modified Redlich-Kwong equation of state, Chem Eng Sci 27 (1972) 1196-1203

[23] NEMESIS2+ website; http://www.nemesis-project.eu/ (accessed 12.08.2015)

[24] I.C. Kemp, Pinch Analysis and Process Integration, Elsevier Ltd (2007), Second Edition

[25] P. Christensen, L. R. Dysert, AACE International Recommended Practice No. 18R-97: Cost estimate classification system – as applied in engineering, procurement, and construction for the process industries, AACE International (2011)

[26] M. Peters, K. Timmerhaus, R. West, Plant design and economics for chemical engineers. McGraw-Hill (2004)

[27] R. Smith, Chemical process design and integration, Wiley (2005)

[28] U.S. Department of Energy, National Energy Technology Laboratory, Technology Learning curve (FOAK to NOAK), Publication number: DOE/NETL-341/081213 (2013)

[29] Access Intelligence, Chemical engineering plant cost index, Chemical Engineering 122 (2015) 63-64

[30] R. D. Stewart, R. M. Wyskida, J. D. Johannes, Cost estimators reference manual, Wiley (1995), Second Edition

[31] Federal Statistical Office of Germany, Statistisches Jahrbuch 2014, Wiesbaden (2014)

[32] Dutch Association of Cost Engineers (DACE), Price Booklet 30 Edition (2014)

[33] Federal Statistical Office of Germany, https://www.destatis.de (accessed 24.07.2015)

[34] Union zur Förderung von Öl - und Proteinpflanzen e.V. (UFOP), Biodiesel ab Tanklager, Großhandelspreise ohne Mehrwertsteuer, http://www.ufop.de/biodiesel-und-co/biodiesel-preis/ (accessed 25.07.2015)

[35] Fachagentur Nachwachsende Rohstoffe e.V. (FNR), Basisdaten Bioenergie Deutschland August 2014